Energy 330 (2025) 136735

Contents lists available at ScienceDirect

Energy

journal homepage: www.elsevier.com/locate/energy

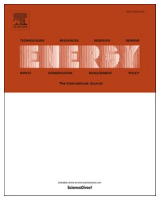

Modeling and optimization of ammonia/hydrogen/air premixed swirling flames for NOx emission control: A hybrid machine learning strategy

Hao Shi [a,b], Zebang Liu [a,*], Syed Mashruk [a], Mohammad Alnajideen [a], Ali Alnasif [a,c], Jing Liu [d], Agustin Valera-Medina [a]

[a] School of Engineering, Cardiff University, Queen's Building, Cardiff, CF24 3AA, United Kingdom
[b] Technical University of Darmstadt, Department of Mechanical Engineering, Reactive Flows and Diagnostics, Otto-Berndt-Straße 3, 64287, Darmstadt, Germany
[c] Department of Aeronautical Techniques, Engineering Technical College of Al-Najaf, Al-Furat Al-Awsat Technical University, Najaf, 31001, Iraq
[d] Center for Reproductive Medicine, Department of Obstetrics and Gynecology, Nanfang Hospital, Southern Medical University, Guangzhou, 510515, China

ARTICLE INFO

Handling editor: P Ferreira

Keywords:
Ammonia/hydrogen combustion
NOx reduction
Nitrogen emissions
Machine learning
Optimization

ABSTRACT

In the face of escalating climate change concerns, the quest for sustainable energy solutions is more pressing than ever. This study delves into the potential of hydrogen and ammonia as alternative fuels, with a focus on ammonia's promise due to its zero-carbon emissions and high energy density. Employing machine learning techniques, specifically XGBoost and SVR, this study presents a comprehensive analysis of ammonia and hydrogen fuel blends to predict NOx emissions and flame temperature with high accuracy, achieving R^2 values predominantly above 0.97. The model's precision is particularly noteworthy compared to other machine learning techniques, where it consistently outperforms with the lowest MSE of 3508.31 and an impressive R^2 value of 0.97653. A detailed feature importance analysis underscores the significance of NH_3 mole proportion, equivalence ratio, and total mass flow rate in influencing nitrogen emissions. Furthermore, the proposed XSN optimization framework has proven effective in reducing nitrogen compounds, achieving a substantial decrease in N-gases concentration by 51.91 %, from 69.81 ppm to 33.57 ppm. The hybrid model developed in this study demonstrates exceptional capability in managing multiple optimization objectives, thereby offering advantages in reducing the overall harmful emissions while maintaining stable operation in practical applications of NH_3/H_2 combustion. This research enhances the accuracy of emissions prediction under diverse conditions and provides valuable insights into effective strategies for controlling nitrogen emissions from NH_3/H_2 combustion.

1. Introduction

According to the International Energy Agency (IEA), the global energy demand is projected to triple in the next decade and quintuple by the mid-century [1]. However, the increasing energy consumption, along with the rising carbon dioxide levels in the atmosphere, poses a serious and complex challenge for humanity. The threat of climate change and global warming urges the transition to a low-emission, carbon-free economy. Therefore, the search for clean and renewable energy sources drives the investigation of alternative non-fossil fuels, such as hydrogen. However, hydrogen as a fuel has inherent challenges of storage and distribution [2,3]. In contrast, ammonia is regarded as a promising candidate for the future energy sector due to its superior properties such as zero-carbon emission, easy storage, high energy density, etc. Furthermore, ammonia in combustion systems is becoming a viable option for replacing fossil fuels and reducing carbon emissions [4,5]. However, the widespread adoption of ammonia as a fuel still faces several challenges, such as its high ignition point, low combustion speed, and temperature constraints under some conditions. These factors lead to unstable ammonia flames, with low flame speed and thick flame structure. In addition, ammonia combustion results in significant NOx emissions due to the fuel-nitrogen atom. These issues limit the feasibility of ammonia as a fuel replacement [6].

To overcome these drawbacks of ammonia-based combustion, ammonia/hydrogen fuel blends have been appraised as a potential solution due to their higher laminar burning velocity, enhanced reactivity [7], and wider flammability limit compared to pure ammonia flames [8]. However, the binary fuel may produce higher levels of NOx than pure ammonia flames because of the high flame temperature and the abundance of O, H, and OH radicals that facilitate fuel NO formation [9,

* Corresponding author.
E-mail address: Liuz91@cardiff.ac.uk (Z. Liu).

https://doi.org/10.1016/j.energy.2025.136735
Received 20 August 2024; Received in revised form 19 April 2025; Accepted 21 May 2025
Available online 22 May 2025

10]. Since NOx emission poses serious threats to human health and eco-environment, considerable efforts are being made to reduce NOx emissions for ammonia/hydrogen combustion, although there are still many unknown phenomena regarding the production of these pollutants. On the one hand, Lee and Kwon [11] reported that the increasing fraction of NH_3 in the blended fuel increased the formation of NO_x and N_2O. On the other hand, Otomo et al. [12] demonstrated that the NO concentration increased with an increase in H_2 mole fraction, mainly due to thermal NOx (i.e., $N + O_2 \rightarrow NO + O$, $N + OH \rightarrow NO + H$). Moreover, operating under fuel-rich conditions was found to be effective in reducing NO concentrations as well as the formation of H_2 from NH_3. Overall, the NOx formation and reduction mechanisms are still not fully understood because of their complexities and variations under different conditions (e.g., reactants, equivalence ratio, pressure, temperature, etc.). Many approaches can be used to reduce NOx emissions, such as operating parameters optimization [13], catalyst adoption [14], humidification [15], and plasma-assisted combustion [16], etc. Among them, the approach of operating parameters optimization, which optimizes the operating parameters by modeling NOx emission and using appropriate optimization algorithms, is more desirable because it is more time and cost-efficient and easier to implement than the other methods. However, due to the nonlinearity of parameter analysis and the multivariability of combustion conditions, coupled with the huge demand for parameter analysis, it poses a huge challenge to the current manual observation and simple statistical analysis methods.

Recently, many machine learning (ML) techniques have been applied to solve these problems, offering a new insight for combustion studies. The machine learning methods enable data-driven techniques for processing large amounts of combustion data, either obtained through experiments or simulations under multiple spatiotemporal scales, thereby discovering the hidden patterns underlying these data and advancing combustion research [17]. Among these techniques, artificial neural networks (ANN) stand out for their capacity for automatic feature extraction, robust nonlinear fitting, and generalization, making them a popular choice for predicting combustion temperatures and pollutant emissions in diverse applications, from IC engines to swirl flames [18, 19]. Despite their advantages, ANNs face challenges such as the need for extensive control parameters, difficulty in achieving stable solutions, prolonged training durations, and a propensity for overfitting, which hampers their broader application [20]. Additionally, the performance of ANN models is contingent upon the adequacy and representativeness of the input data [21].

Random forest (RF) [22], while valuable, has shown limitations in measurement accuracy within combustion estimation studies [23]. Similarly, decision tree (DT) models require laborious data preprocessing when handling voluminous combustion data sets [24]. The advent of eXtreme Gradient Boosting (XGBoost) represents a paradigm shift, amalgamating the strengths of various algorithms to address the deficiencies of traditional ML techniques [25]. The efficacy of XGBoost in constructing single-target prediction models for NOx emissions has been demonstrated, indicating its potential utility in combustion research [26]. Comparative studies by Li et al. [27] have highlighted the computational efficiency and predictive accuracy of XGBoost over other algorithms like RF and KNN. Dong et al. [28] leveraged XGBoost to develop predictive models for NOx emissions and pressure fluctuations in gas turbines, showcasing the precision of the algorithm. Yao et al. [29] employed XGBoost and Light Gradient Boosting Machine (LGBM) to model the filtered density function (FDF) of mixture fractions in turbulent evaporating sprays, achieving accuracy levels comparable to deep neural networks.

Support vector regression (SVR) has emerged as a computational intelligence-based method designed to surmount the limitations of ANN and offer superior solutions for highly nonlinear problems [30]. The attempts to apply SVR in modeling NOx emissions from coal-fired boilers have yielded promising results, with a closer alignment between predicted and actual emission concentrations [21]. Although XGBoost adeptly manages non-linear relationships, it lacks the non-linear fitting prowess of SVR, particularly in high-dimensional feature spaces, the use of SVR in isolation for nonlinear relationships necessitates expert selection of kernel functions, which is not easy to determine. Therefore, this study proposes a combined XGBoost and SVR approach to enhance model robustness and generalization capabilities while mitigating overfitting risks. Compared to previous studies on predicting NOx emissions, the proposed hybrid machine learning methodology is highly effective in handling the multivariable nature of combustion conditions and large dataset, addressing nonlinear challenges, and enabling more accurate predictions of combustion emissions. This robust method holds substantial promise for advancing the sustainable development of renewable energy sources [31].

ML methods have increasingly been recognized for their efficacy in optimizing combustion emissions, such as the extreme learning machine [32] and deep neural network [33]. However, these techniques often exhibit constraints, particularly when addressing multi-objective optimization problems, due to their inherent single-objective focus and the complexity of their models [34]. To address these limitations, we employed the Non-dominated Sorting Genetic Algorithm II (NSGA-II), renowned for its elite retention strategy, rapid non-dominated sorting, and crowding distance calculation, facilitating the swift acquisition of high-quality Pareto-optimal solution sets [35,36]. This study pioneers a multi-objective optimization framework, integrating advanced machine learning models, to offer a novel approach for comprehending and mitigating nitrogenous emissions (NO, NO_2, N_2O, and NH_3) during the NH_3/H_2 combustion process. The proposed framework facilitates intelligent optimization of model parameters through genetic operations such as crossover, mutation, and selection. By iteratively refining parameter combinations, the algorithm adeptly navigates conflicting objectives to identify optimal operating conditions. This process not only yields the most favorable outcomes but also provides a robust, data-driven foundation for the design of efficient burners.

In this study, the XGBoost and SVR are first employed to construct a predictive model for NOx&NH_3 emissions and adiabatic flame temperatures (AFT) of ammonia/hydrogen combustion in a swirl burner. The predictive performance of the established models is evaluated against other machine learning techniques. Next, a comprehensive feature importance analysis is conducted to discern the predominant factors (e.g., NH_3 mole fraction, equivalence ratio, thermal power) influencing the emissions from the NH_3/H_2 swirling flame, thereby elucidating the underlying flame chemistry. Furthermore, this study introduces an optimization framework aimed at reducing nitrogen compounds (NO, NO_2, N_2O, and NH_3) by fine-tuning operational parameters. The predictive capabilities of the established model enable accurate predictions and optimizations of NOx and NH_3 emissions, under diverse operational conditions. This research furnishes valuable insights into the flame chemistry associated with NOx emissions and proffers viable strategies for emission reduction in NH_3/H_2 combustion processes. The paper is structured as follows: Section 2 delineates the experimental setup, chemical modeling methods, and dataset used for ML training; Section 3 details the machine learning models, their training and evaluation protocols, and the proposed multi-objective optimization framework; Section 4 presents the empirical findings, including the impact of the predictive model, the salience of each parameter, and recommendations for minimizing NOx and NH_3 emissions; Section 5 culminates with the key findings and implications of the study.

2. Experimental setup and data acquisition

2.1. Swirl burner and operating conditions

The experimental investigations were executed utilizing an industrial-scale tangential swirl burner, delineated by a geometric swirl number of $S_g = 1.05$. A schematic delineation of the experimental apparatus is depicted in Fig. 1. The burner comprised a radial-tangential

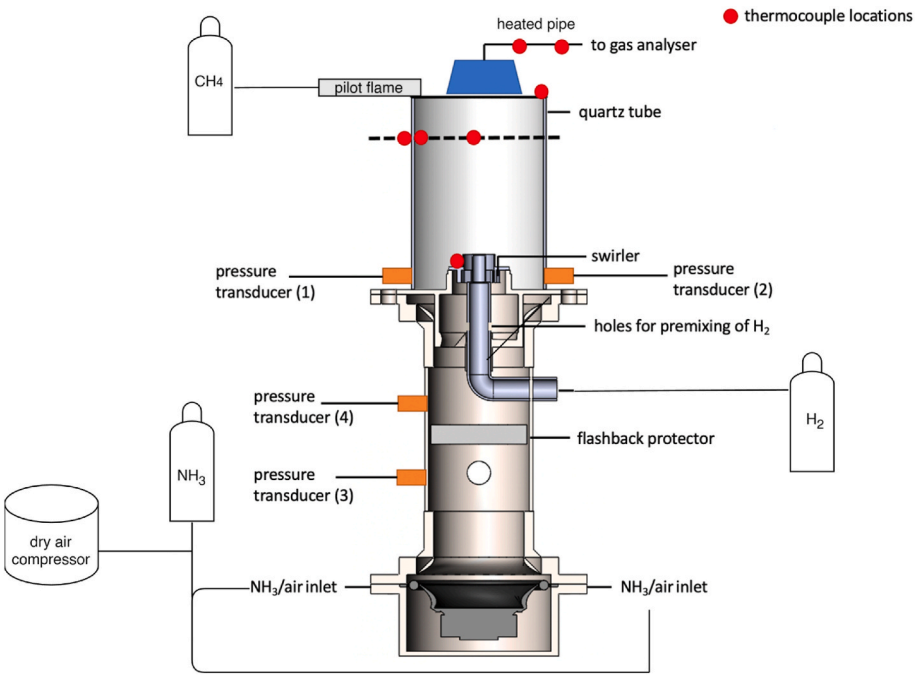

Fig. 1. Tangential combustor with measuring techniques and control systems.

swirler integrated with a central bluff body (22.5 mm diameter) to stabilize the flame and enhance mixing uniformity. A transparent cylindrical quartz confinement tube (156 mm diameter) provided optical access for chemiluminescence imaging and spectroscopic diagnostics, as detailed in Ref. [37]. A comprehensive range of ammonia/hydrogen mixtures was scrutinized, spanning a wide array of equivalence ratios (∅), all conducted under standard atmospheric conditions (T_{in} = 288 ± 5 K, P_{in} = 0.11 ± 0.005 MPa). The system was calibrated to sustain a steady outlet pressure P_{out} = 0.11 ± 0.005 MPa. Ammonia and air were channeled into the mixing chamber from its base, while hydrogen was methodically introduced through six equidistant radial orifices, each with a diameter of 1.5 mm, positioned on the central lance, 40 mm below the burner exit. These orifices were strategically angled at 45° to promote the direct injection of hydrogen into the swirling current, thus ensuring an exhaustive premixing with ammonia and air before combustion. The volumetric flow rates of the reactants were precisely modulated using Bronkhorst mass flow controllers, which boast an accuracy of ±0.5 % within a mass flow range of 15–95 %. A permanent methane pilot flame was integrated to assist ignition and prevent blow-off during transient conditions [38].

In the present study, three distinct datasets were meticulously curated to underpin the establishment and training of the predictive model, each dataset reflecting a unique set of operational conditions. The parameters selected for investigation—namely, the equivalence ratio (ER), thermal power, ammonia mole fraction (X_{NH_3}), and the Reynolds number—are exhaustively cataloged in Table 1. The total mass flow was defined as the total mass flow rate of the premixed air/fuel reactants. The Reynolds number, a dimensionless quantity characterizing flow regime, was calculated using Eq. (1):

$$Re = \frac{\rho u D}{\mu} \tag{1}$$

where ρ is the density of the premixed air/fuel flow, and the μ is the dynamic viscosity of the premixed flow calculated by an online transport properties calculator [39], u is the mean burner exit nozzle velocity, and D is the nozzle diameter.

This table also quantifies the number of data groups encapsulated within each dataset, providing a clear overview of the data structure and diversity. These datasets are pivotal in facilitating the machine learning model to generalize and accurately predict NOx emissions under a variety of combustion scenarios.

The ammonia mole fraction (X_{NH_3}) in the ammonia/hydrogen binary fuel is defined as follows:

$$X_{NH_3} = \frac{[NH_3]}{[NH_3] + [H_2]} \tag{2}$$

where $[NH_3]$ and $[H_2]$ represent moles of ammonia and hydrogen, respectively.

2.2. Emissions

Exhaust emissions such as NO, N_2O, NO_2, NH_3, O_2, and H_2O, were quantified utilizing a specialized quantum cascade laser analyzer (Emerson CT5100). The apparatus operated at an elevated temperature of 463 K and a sampling frequency of 1 Hz, ensuring a high-fidelity temporal resolution. The measurement system demonstrated an accuracy of ±1 % and an exemplary linearity of 0.999, indicative of the precision of the analytical technique employed. A dilution methodology was integrated into the experimental protocol, wherein N_2 was

Table 1
Comprehensive synopsis of experimental parameters employed in the dataset.

Dataset	ER	Thermal Power (kW)	X_{NH_3} (vol%)	Reynolds Number	Total Mass Flow (g/s)	Number of Data Groups
A	0.65	10, 15, 20	50–100 (5 inc.)	8927–19234	5.11–10.95	28
B	0.6–1.4 (0.05 inc.)	8	70, 75, 85, 95, 100	3711–8996	2.32–4.61	33
C	0.65	10	50–95 (5 inc.)	3450, 5175, 6900	4, 6, 8	29

introduced into the exhaust sample via a Bronkhorst EL-FLOW Prestige MFC. This MFC facilitated the pre-heating of nitrogen to 160 °C before its amalgamation with the exhaust gases, thereby ensuring a consistent sample state. The flow rate of the exhaust sample (F_S) during the dilution process was meticulously calculated, taking into account the total intake flow rate (F_t) and the dilution nitrogen flow rate (F_d), as explicated in Eq. (3):

$$F_S = F_t - F_d \tag{3}$$

An isokinetic funnel, featuring an intake diameter of 30 mm, was meticulously aligned 50 mm downstream from the terminus of the quartz confinement. This configuration was engineered to procure homogenous samples from the effluent stream, tailored to specific operational regimes. Samples were transported through a heated line (463 K) to prevent condensation and analyzed in real time. The emission metrics delineated in this document were methodically aggregated and averaged across a temporal span of 120 s.

2.3. Chemical modelling

To elucidate the influence of variable conditions on the emission profiles, an exhaustive chemical analysis was performed using the Ansys CHEMKIN-PRO platform. This analysis centered on the analysis of AFT within swirling turbulent flames under diverse operational scenarios. Utilizing the PREMIX module within the CHEMKIN-Pro package, the simulation of a one-dimensional adiabatic planar flame was executed, advancing our understanding of reactivity trends. The adopted model incorporates the reaction mechanism proposed by Stagni et al. [40], which has been corroborated by recent studies [41,42] for its efficacy in simulating NH_3/H_2/air combustion. This mechanism encompasses 31 chemical species and 203 reactions.

3. Methodology

As illustrated in Fig. 2, in this study we present a novel machine learning algorithm that exhibits exceptional proficiency in fitting and forecasting the multifaceted attributes of combustion phenomena, alongside a spectrum of emission and output parameters. The datasets detailed in Tables 1 and in conjunction with the corresponding emissions and AFT for each case, were pivotal in the formulation and corroboration of the computational models. The dataset was methodically partitioned into a training set (comprising 80 % of the samples) and a test set (encompassing the remaining 20 %). The training set laid the groundwork for the model construction, while the test set was employed to evaluate the predictive accuracy of the model.

This innovative algorithm has undergone a comprehensive comparative analysis against a suite of established algorithms, including ANN, as well as an array of hybrid methodologies (e.g., RF, RF + Linear Regression). The empirical results from these comparative studies underscore the algorithm's enhanced performance, outstripping its counterparts in terms of effectively steering emission levels and optimizing combustion conditions.

3.1. XGBoost

XGBoost emerges as a forefront machine learning methodology, materialized through an advanced optimization framework as delineated by Chen and Guestrin [43]. This technique is anchored in the principles of gradient boosting decision trees (GBDT), systematically combining weak learners in a sequential ensemble. It incorporates a regularization term in its objective function to effectively mitigate overfitting. This feature makes XGBoost particularly advantageous for applications involving limited datasets.

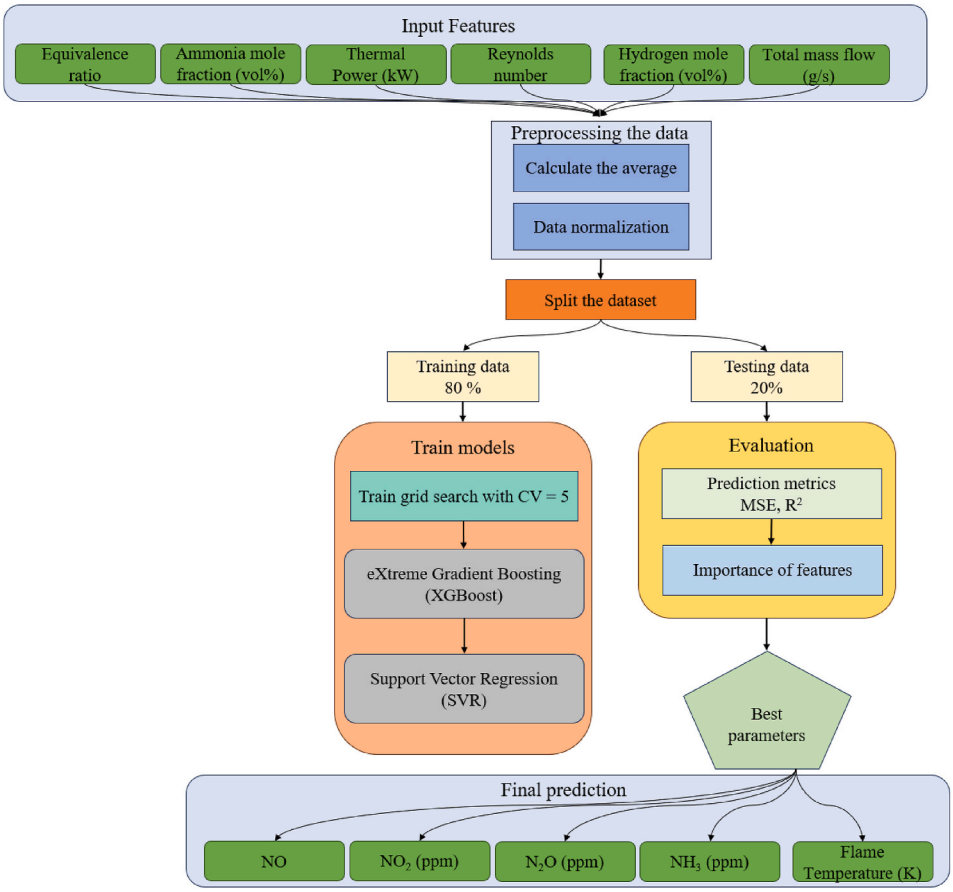

Fig. 2. Conceptual framework of the proposed machine learning algorithm.

In the preliminary stage of the hybrid modeling approach, an XGBoost model was meticulously trained on the designated dataset. This model adeptly captured complex nonlinear patterns and interactions among variables by constructing multiple decision trees and optimally combining their predictions. The parameters governing the XGBoost model are systematically enumerated in Table 2. The objective function of the XGBoost model was bifurcated into two distinct components: an error function term L and a model complexity function term Ω. The objective function is written as [43]:

$$Obj^{(r)} = \sum_{i=1}^{n} L\left(y_i, \hat{y}_i^{(r)}\right) + \sum_{i=1}^{r} \Omega(g_r) \tag{4}$$

where.

y_i - real value, $\hat{y}_i^{(r)}$ – the prediction at the r-th round, g_r -the structure of the decision tree, $L\left(y_i, \hat{y}_i^{(r)}\right)$ - Loss Function, n – the quantity of training examples, $\Omega(g_r)$ – regularization term.

3.2. SVR model

After the training phase of the XGBoost model, the resultant predictive values were employed as input features to calibrate a series of SVR models, each meticulously tailored to predict distinct output variables. The SVR technique, an extension of the Support Vector Machine framework, is proficient in executing both linear and non-linear regression tasks. Contrary to the conventional SVM classification approach, the SVR methodology aspires to identify an optimal hyperplane that minimizes the deviation of all training samples, ensuring the narrowest margin from the extremal data points, as depicted in Fig. 3. These SVR models play a pivotal role in unraveling the complex nonlinear dependencies that exist between the input features and the corresponding outputs. In instances where the dataset exhibits non-linear characteristics, kernel functions are utilized to transmute the feature space, mirroring the SVM strategy, and subsequently facilitating the regression analysis [44].

In divergence from the SVM classification schema, SVR aimed to construct an optimal hyperplane that fits all training samples, maintaining a minimal distance from the outermost training data. Fig. 3 delineates the schematic representation of the SVR mechanism. The SVR models were instrumental in elucidating the intricate non-linear correlations between the inputs and outputs. For dataset that present nonlinear fitting challenges, kernel functions were invoked to remap the feature space, analogous to the SVM technique, preceding the execution of the regression [44].

As explicated in Table 3, a judicious selection of parameters is instituted for the SVR models. Each model was subjected to a training process to align the forecasts derived from the XGBoost model with the respective output variables.

3.3. Grid search

In the current investigation, we scrutinized two prominent machine learning classifiers: XGBoost and SVR. These classifiers were trained to ascertain the optimal hyperparameters and configurations, leveraging a robust estimation methodology. The Python Scikit-Learn library offered a streamlined grid search mechanism, facilitating the meticulous optimization of hyperparameters for each classifier. This process was instrumental in deriving configuration parameter recommendations that

Table 2
The hyperparameters search range of the XGBoost model.

Number of estimators	[20, 40, 60, 80, 100, 120]
Maximum depth	[10, 30, 50, 80, 100]
Learning rate	[0.1, 0.2, 0.3, …, 0.9]

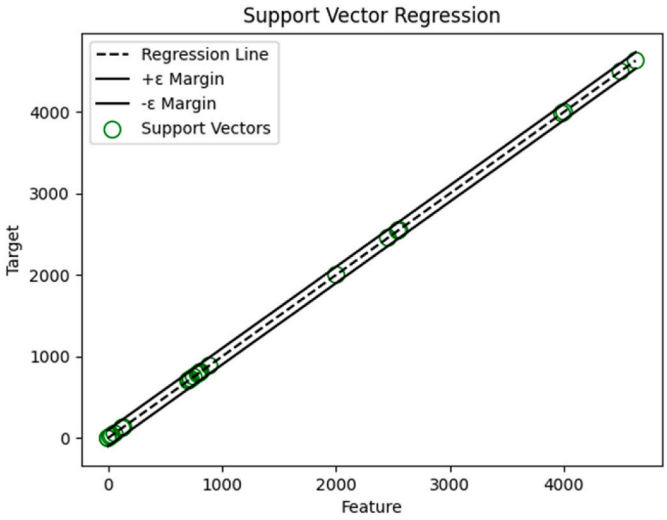

Fig. 3. Schematic diagram of SVR.

Table 3
The hyperparameters search range of the SVR model.

Kernel	[1, 2, 4, 6]
Regularization parameter C	[20, 60,100]
Degree	[1, 2, 3, 4, 5, 6]
Kernel	[1, 2, 4, 6]

are tailored to the algorithm in question. Throughout the hyperparameter tuning phase, the most efficacious combinations of hyperparameters for both models, as determined through a random search, are systematically cataloged in Tables 4 and 5.

3.4. The NSGA-II algorithm

Among various optimization algorithms, the NSGA-II was selected for its proven efficiency in handling multi-objective problems with high-dimensional data [45]. The ability of NSGA-II to identify a diverse set of Pareto-optimal solutions was particularly advantageous for our study, which aimed to balance multiple emission objectives without compromising computational speed. Consequently, the NSGA-II framework was employed as a pivotal multi-objective optimization method in this study to reduce nitrogen emissions while maintaining stable AFTs.

As illustrated in Fig. 4 and detailed in Table 6, our optimization strategy intricately combined the predictive capabilities of XGBoost and SVR models within the NSGA-II algorithmic structure. This innovative configuration began with the generation of an ensemble of candidate solutions, denoted by N, each evaluated for fitness based on the predictive accuracy of the combined XGBoost-SVR model suite.

The optimization process began with the initialization of the population. The XGBoost-SVR model selects the input variables most likely to influence NOx emissions and flame temperature, generating a series of high-quality candidate solutions from the outset. The fitness function was calculated using the SVR model, with each solution's performance evaluated based on the prediction results of the XGBoost model. Specifically, the parameters of each candidate solution were first processed and predicted by the XGBoost model, with the prediction results

Table 4
The optimal hyperparameters of the XGBoost model.

Number of estimators	100
Maximum depth	50
Learning Rate	0.6
Objective	Regression with squared error loss

Table 5
The hyperparameters of the SVR model.

Kernel	4
Regularization parameter C	100
Degree	4
Coefficient for the polynomial kernel function	1
Gamma	Scale

subsequently used as input to the SVR model, defining and evaluating the fitness function.

Following the primary non-dominated sorting phase, a new generation of solutions was derived through fundamental genetic algorithmic processes: selection, crossover, and mutation. These genetic operations generated a new generation of candidate solutions, enhancing the ability of the algorithm to explore the solution space and maintain genetic diversity. From the subsequent generation onward, a rapid non-dominated sorting was applied to the combined set of ancestors and their successors. Concurrently, the crowding distance metric was calculated for each solution within the non-dominated strata. This metric, along with the non-dominated ranking, guided the selection of the most promising candidates, fostering the development of a new ancestral lineage.

The proposed XGBoost-SVR-NSGA-II (XSN) framework, integrating multiple machine learning techniques, served not only as an optimization tool but also as a complex decision support system. This methodical approach ensured a judicious balance between exploration and exploitation within the solution space, ultimately aiming to achieve a Pareto-optimal set. This set was characterized by its ability to minimize NOx emissions while concurrently maintaining the AFT within predefined

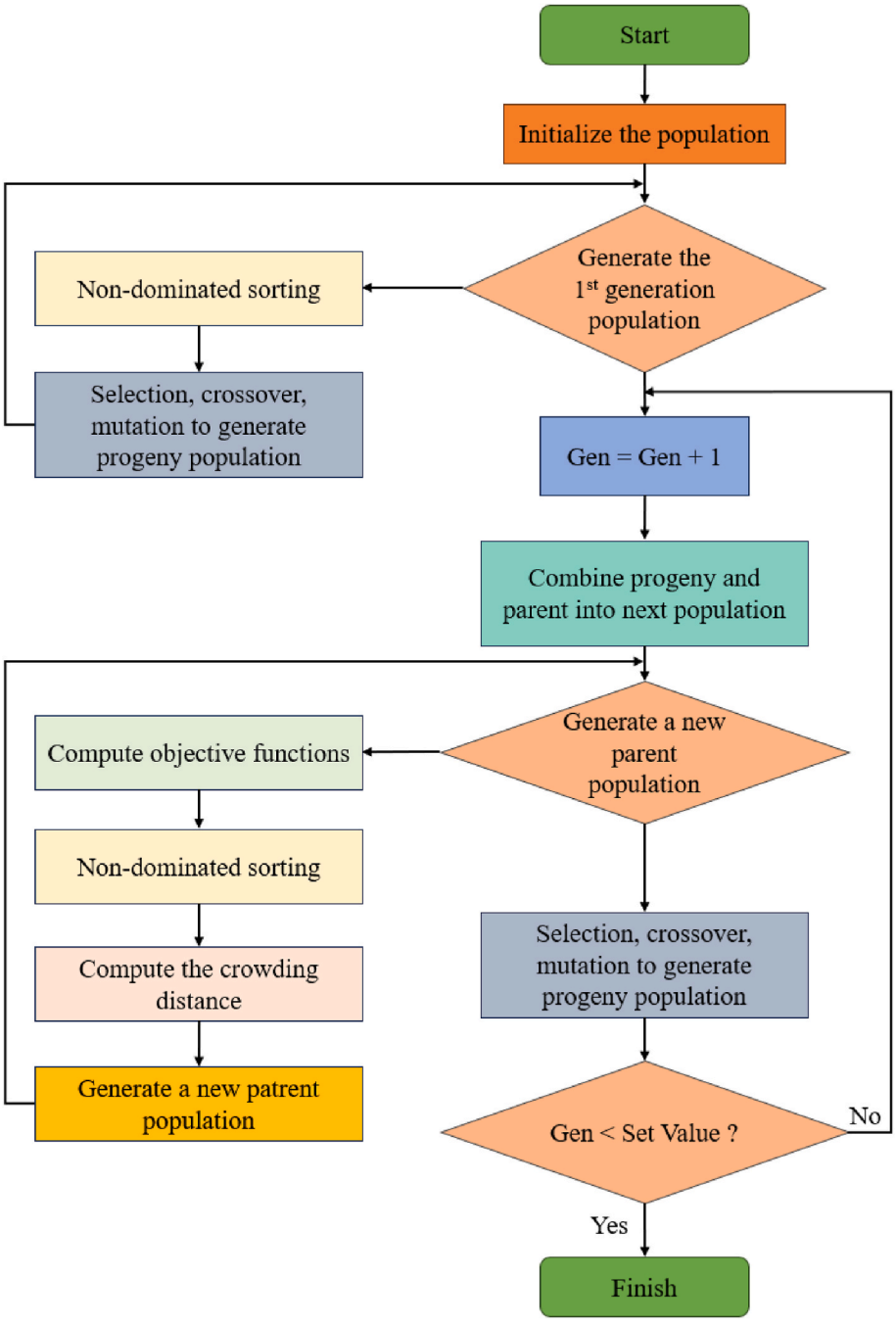

Fig. 4. Computational flowsheet of the XSN framework.

Table 6
The procedure of the NSGA-II algorithm.

NSGA-II Procedure
Input: N, T, F_k (X) ▷ N members evolved T generations to solve Min f_k (X)
Initialize Population P_0 size N randomly;
for $t = 1$ to T do:
Generate next offspring population Q_t size N by:
Binary Tournament Selection;
Crossover and Mutation;
Combine current Parents P_t and new offspring Q_t to form R_t;
Calculate objective values for R_t;
Assign Rank (level) for R_t; based on Pareto fronts F_k (non-dominated solutions);
Calculate Crowding distance (CD) for each solution in R_t;
Initialize next Parent population P_{t+1} by the following loop:
Add solutions in lowest rank Pareto fronts with priority for a greater CD until getting N individuals are obtained;
End

constraints.

3.5. Metrics

In the assessment of the regression model performance, the Mean Square Error (MSE) was employed as a fundamental metric. The MSE quantifies the average of the squares of the errors, essentially capturing the variance between the predicted values and the observed data points. This metric serves as a lucid gauge of the model's precision and predictive accuracy.

$$\mathrm{MSE} = \frac{1}{m}\sum_{i=1}^{m}(X_i - Y_i)^2 \tag{5}$$

Furthermore, the Coefficient of Determination (R^2), a non-dimensional index, was utilized to evaluate the fit of the model. An R^2 value approaching unity is indicative of a model that accounts for a greater proportion of the variance observed in the dependent variable, suggesting a robust correlation between the independent variables and the dependent variable. The proximity of the data points to the regression line, reflected by a higher R^2 value, denotes a denser clustering of observations and, consequently, a model that more adeptly elucidates the variability of the data.

The R^2 value is calculated as follows:

$$R^2 = 1 - \frac{\sum_{i=1}^{m}(X_i - Y_i)^2}{\sum_{i=1}^{m}(\overline{Y} - Y_i)^2} \tag{6}$$

where.

X_i - the predicted output value of sample i,
Y_i - the actual output value of sample i,
$\overline{Y}$ - the mean value of samples Y_i (i = 1, 2, …, m).

The MSE, with its range extending from 0 to $+\infty$, operates as an indicator of prediction accuracy; a diminutive MSE value denotes a model that more precisely mirrors the observed data. In contrast, the R^2 values are confined within the interval (0, 1), where an elevated R^2 value signifies a model endowed with enhanced predictive capabilities.

3.6. Features importance

In our research, Feature Importance (FI) was employed as a statistical metric to quantify the contributory weight of input features on the predictive outcomes of the model. An elevated FI value was indicative of the heightened impact of a feature on the model output. A comprehensive assessment of feature importance was undertaken within the model framework to identify the critical factors that significantly influence the prediction of emissions and flame temperatures. The input features subjected to this evaluation are enumerated in Table 7.

The FI values were computed using a perturbation-based method, also known as permutation importance. This approach is widely adopted as a model-agnostic method for global explainability [22]. FI analysis offered a window into the model's internal mechanics, identifying the variables with the most significant impact on the prediction objective. This analysis was pivotal in honing the model—by eliminating less influential features, the model's computational efficiency was enhanced and the risk of overfitting is mitigated, both of which were essential for the model's practical application.

In this study, the FI for both individual XGBoost models and their composite counterparts were presented. Within the individual XGBoost model, the importance value of each feature was ascertained based on the frequency of its utilization as a split node. The importance of a feature was calculated by calculating the total number of split points for each feature in the model, alongside the extent to which each split point improves model performance. The higher the feature importance value, the greater the contribution of the feature to the model's predictive ability. For each feature x_j in the model, its importance I_j is calculated by:

$$I_j = \frac{1}{M}\sum_{m=1}^{M}\left(\sum_{t=1}^{Tm}\left(\widehat{i}_{jt}^{\,2}\cdot 1(v(t)=j)\right)\right) \tag{7}$$

where.

M − the total number of trees in the model,
Tm -the set of all non-leaf nodes of the m-th tree,
$v(t)$ - split variable associated with node t,
$\widehat{i}_{jt}^{\,2}$ - the square error improvement obtained by using variable x_j as the splitting variable at node t
$1\ (v(t)=j))$ - an indicator function whose value is when node t uses feature x_j as the splitting variable, and is 0 otherwise. This formula encapsulates the process where, for each tree within the ensemble, the x_j is used as the sum of $\widehat{i}_{jt}^{\,2}$ that splits the node. This sum is then normalized by the total number of trees (M) in the model to yield the average importance I_j of feature x_j.

The permutation importance method was employed to discern the significance of features within the composite model post-XGBoost application. This method quantified the contribution of each input feature by measuring the degradation in model performance when the feature's values are randomly shuffled, thereby breaking its association with the output, and its formula is expressed as follows:

$$FI_j = \frac{1}{N}\sum_{n=1}^{N}\left(MSE_{Original} - MSE_{Permuted_j}\right) \tag{8}$$

where.

FI_j - The importance of the j-th feature;
N – The number of times to repeat the substitution;
$MSE_{Original}$ - The mean square error of the original data and the above model prediction;
$MSE_{Permuted_j}$ - The mean square error of model predictions after permuting the j-th feature.

Table 7
Input features.

1. Equivalence ratio	4. H_2 ratio (vol%)
2. Thermal Power (kW)	5. Re
3. NH_3 ratio (vol%)	6. Total mass flow (g/s)

The specific steps feature importance evaluation are as follows.

a. Training Phase: The composite model is trained using the original dataset to establish a baseline metric for predictive performance.
b. Perturbation Phase: Values of a particular feature are randomly permuted across the dataset, generating a perturbed variant.
c. Prediction Phase: This altered dataset is then employed to predict outcomes, from which a permutation performance score is derived.
d. Impact Assessment: The feature's influence is quantified by the discrepancy between the baseline and permutation scores, indicative of the feature's importance ranking.
e Normalization: Importance rankings across all features are normalized to sum to unity, yielding the relative importance ratio for each feature.

Through this structured process, we quantitatively determined the contribution of individual features to the model's predictive accuracy. This elucidation not only highlighted the significance of each feature within the composite model but also informed strategic feature selection to optimize model performance.

3.7. System optimization using XSN architecture

In the pursuit of reducing nitrogen oxide emissions while concurrently stabilizing flame temperature, this study introduced a multi-objective optimization framework. While conceptually related to the optimization tool developed by Zhou et al. [46], which prioritized NOx emission reduction and demonstrated robustness concerning control parameters, our framework extended this prior work by explicitly incorporating flame temperature stabilization as a concurrent objective. Central to this framework was a machine learning model leveraging the XGBoost-SVR algorithm to construct the fitness function integral to the optimization process. Input features, as delineated in Table 1, were sampled within their respective operational ranges as established by experimental design. The multi-objective optimization framework is governed by two principal objectives.

i) Minimize NOx&NH_3 emissions.

$$\min NO_x = f_{NO}(x) + f_{NO_2}(x) + f_{N_2O}(x) + f_{NH_3}(x) \quad (9)$$

ii) Maintain flame temperature within 1600K–2100K: This temperature range is essential for the efficient operation of combustion equipment and for ensuring the stable convergence of the optimization algorithm.

Where:

$f_{NO_x}(x)$ denotes the predictive model for NOx emissions, and $f_{Temp}(x)$ represents the predictive model for flame temperature, both as functions of the input parameters. The optimization process aimed to identify a parameter set that not only minimizes NOx emissions but also maintains flame temperature within the specified range. Temperature difference was defined as the minimum difference of the flame temperature to the allowed range (1600–2100 K) – thus it was zero when the temperature is within the range, and grew if the temperature was too low or too high relative to this band. This dual objective served to mitigate the environmental impact of NOx pollutants while preserving the stable operation of the combustion system.

4. Results and discussion

4.1. Performance of the prediction model

Based on the established XGBoost + SVR model, the comparisons between the predicted results and the measured data of the output features are presented in Fig. 5. Each subplot within the figure delineates the congruence of predicted results with measured data, where the solid line denotes the ideal scenario of error-free prediction. The scatter of data points, representing model predictions, is observed to cluster near this line of perfect agreement. To ensure the reliability of the results, the model's generalizability is evaluated using five-fold cross-validation. The dataset is randomly divided into 5 groups, and used 4 groups (72 experimental groups)to train the model and 1 group (18 experimental groups) to evaluate it. Each experimental group represents a 120-s time average (see Section 2.2 for details). Fig. 5 shows the test set results of one of the folds of cross-validation.

The MSE and R^2 values of each predicted output feature are listed in Table 6. The R^2 values for the output parameters predominantly exceed 0.97, underscoring the excellent prediction accuracy of the established model. An exception is noted in the R^2 value for NO_2 emissions, which stands at 0.934 within the test set. This deviation is potentially attributable to the more dispersed distribution of NO_2 concentrations and their comparatively lower magnitude. Overall, the alignment of predicted results with measured values corroborates the model validity, reinforcing its utility in NOx emission studies pertaining to ammonia/hydrogen combustion.

In the assessment of the hybrid XGBoost + SVR model, a phased training methodology was adopted to scrutinize the convergence of the Root Mean Squared Error (RMSE) throughout the simulated epochs. For the XGBoost component, each epoch signifies a successive iteration over the dataset, progressively honing the ensemble of decision trees. In contrast, the SVR model simulates epochs by incrementally enlarging the dataset, thereby enriching the model's exposure to diverse data points. To facilitate a comprehensive understanding of the model fitting dynamics, both the SVR and XGBoost algorithms were segmented into 50 and 100 epochs, respectively, for illustrative purposes in Fig. 6. Post each epoch, the RMSE metrics were computed for both the training and validation sets, shedding light on the learning trajectory and the generalization aptitude of each constituent within the hybrid architecture. This systematic approach elucidates the distinct and collective proficiency of XGBoost and SVR in the context of predictive modeling for N-gas emissions (NO, NO_2, N_2O, and NH_3). Within the XGBoost algorithm, each epoch signifies a successive iteration over the dataset, facilitating the progressive refinement of the decision tree ensemble. In contrast, the SVR model simulates epochs through a gradual augmentation of the training dataset, thereby permitting the observation of performance enhancements as the model assimilates an expanding corpus of data. After each epoch, RMSE metrics are computed for both the training and validation dataset, yielding insights into the learning trajectory and the generalization aptitude of each algorithmic component within the hybrid construct. This deliberate and methodical evaluation serves to elucidate the individual and synergistic contributions of XGBoost and SVR to the overarching predictive modeling endeavor. Both the empirical evaluations of the XGBoost and SVR models reveal remarkable reductions in the test RMSE across the epochs.

The proficiency of the established model in predicting various emissions and AFT is quantitatively assessed and presented in Table 8. The R^2 and MSE serve as the principal metrics for evaluating model performance. As delineated in Table 8, the R^2 and MSE values, computed for both the training and testing phases, affirm the robust explanatory power and consistent predictive performance of the model. Notably, the R^2 values approximate unity for flame temperature and NH_3 emission during the training phase and remain elevated during testing, validating the model's precision and reliability in these specific predictions. On average, the model exhibits commendable predictive capabilities, with R^2 values of 0.99379 in training and 0.97653 in testing.

Table 9 demonstrates the comparisons of the prediction performance between the XGBoost + SVR and other commonly used models, including the RF, ANN, RF + Linear Regression, RF + ANN, etc. Similarly, the comparative analysis of various models was grounded on MSE and R^2 metrics, key indicators of model accuracy and predictive power.

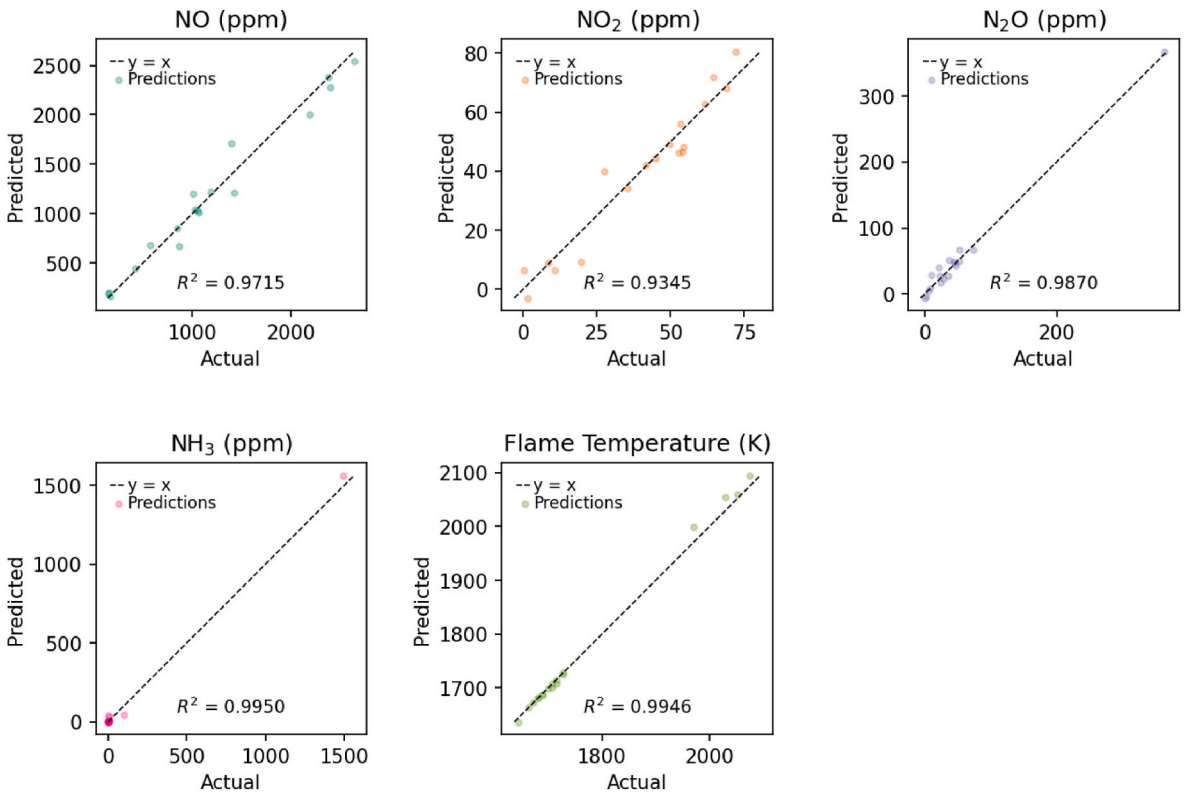

Fig. 5. Comparative analysis of model predictions and empirical data in ammonia/hydrogen flames.

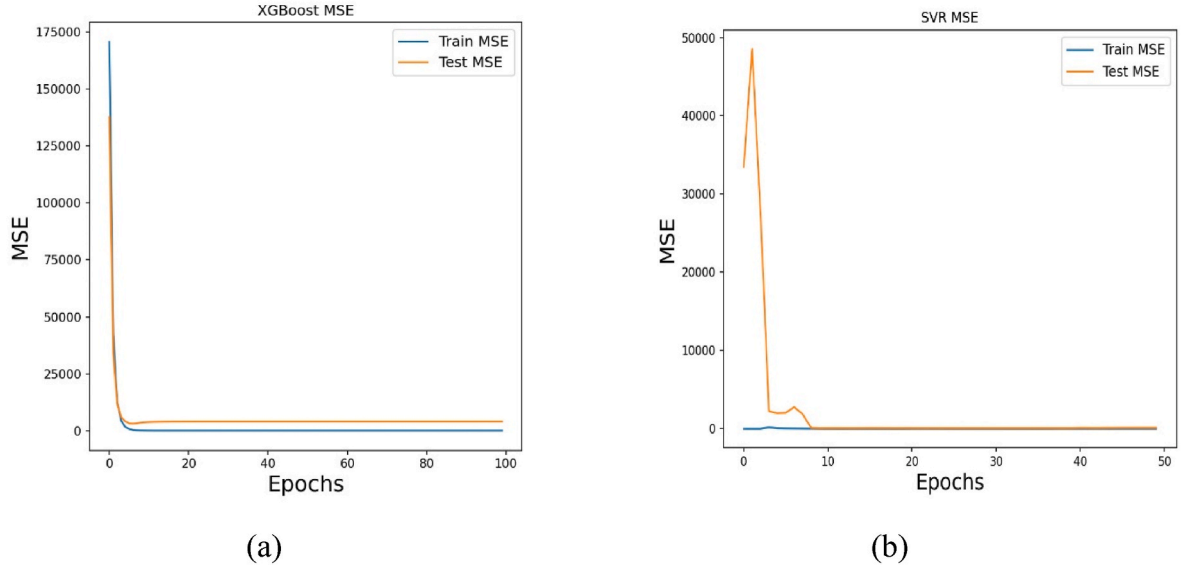

Fig. 6. RMSE convergence across simulated epochs of employed machine learning models. ((a) XGBoost; (b) SVR.

Table 8
Prediction performance of the established model across training and testing phases.

	NO (ppm)	NO_2 (ppm)	N_2O (ppm)	NH_3 (ppm)	Flame Temperature (K)	Average
Train R^2	0.99986	0.98123	0.99057	0.99753	0.99976	0.99379
Train MSE	149.731	36.7810	71.5952	253.801	5.64498	103.511
Test R^2	0.97151	0.93448	0.98704	0.99502	0.99461	0.97653
Test MSE	16738.9	33.8141	81.0623	577.581	110.179	3508.31

Table 9
Comparisons of the prediction performance of different models.

Methods	MSE	R^2
Random Forest	11627.6	0.87160
ANN	46701.8	0.63127
AdaBoost	9477.83	0.79709
RF + Linear Regression	10394.0	0.84544
RF + ANN	77828.3	0.77712
XGBoost	5893.57	0.84646
XGBoost + SVR	3508.31	0.97653

As is shown, the established model of this study (XGBoost + SVR) showcases outstanding performance with the lowest MSE of 3508.31 and the highest R^2 value of 0.97653. This hybrid model significantly outstrips the other contenders, including standalone models and other ensemble techniques. For context, the standalone RF model achieved an R^2 of 0.87160 with an MSE of 11627.6, whereas the ANN scored an R^2 of 0.63127 with a substantially higher MSE of 46701.8. AdaBoost, another ensemble technique, delivered an R^2 of 0.79709 and an MSE of 9477.83. Combining RF with Linear Regression resulted in an R^2 of 0.84544 and an MSE of 10394.0, whereas coupling RF with ANN produced an R^2 of 0.77712 but with a significantly elevated MSE of 77828.3. The standalone XGBoost model offered a competitive R^2 of 0.84646 with an MSE of 5893.57. It can be concluded that the XGBoost + SVR model established in this paper is competent to predict the concentration of NOx emissions (NO, NO_2, N_2O) and flame temperature.

The superior performance of the XGBoost + SVR model can be attributed to its dual capability of capturing complex data patterns. XGBoost can effectively capture the variance in the data, while SVR can model the residuals with its flexible non-linear kernel. The combination of these two models harnesses their respective strengths: the robustness of XGBoost to overfitting and the powerful prediction of SVR of continuous outcomes. The high MSE observed with the RF + ANN model suggests that while ANN added complexity to the model, it did not translate to an improved prediction on this particular dataset, possibly due to overfitting or an inadequate architecture for the data complexity. The standalone underperformance of ANN could be attributed to similar reasons and highlights the challenges of tuning ANNs to specific dataset. In contrast, the low MSE and high R^2 of the XGBoost + SVR model indicate not only a good fit but also a strong generalization capability. The ability of this model to accommodate the variance of the data while also capturing intricate patterns that may be missed by other models sets a new benchmark for predictive accuracy in this application domain.

4.2. Feature importance

In this study, feature importance (FI) is calculated using a perturbation-based method. Specifically, each feature was randomly permuted multiple times across the dataset, and the resulting increase in prediction error (measured by MSE) is averaged. The mathematical formulation is given in Equation (8). The values plotted in Fig. 7 represent the unnormalized FI values, which directly quantify the increase in MSE caused by destroying the association between each input feature and the target. These FI values were not scaled or normalized, and hence reflect the absolute magnitude of feature contribution. The analysis reveals a pronounced sensitivity of NO emissions to the equivalence ratio, corroborating the findings of antecedent studies that the equivalence ratio can substantially impact the NO emissions. Furthermore, the heatmap indicates a significant propensity for ammonia slip under rich NH_3/H_2 combustion conditions, attributable to the concomitant reduction in available oxygen [47]. This phenomenon is underscored by the heightened sensitivity of NH_3 emissions to the NH_3 ratio, accentuating its pivotal role in emission control strategies. The thermal power is observed to exhibit minimal sensitivity to emissions when juxtaposed with the NH_3 ratio and equivalence ratio. Notably, the H_2 ratio is shown to have negligible sensitivity to all emissions and the AFT, a manifestation of its inherent redundancy relative to the NH_3 ratio within the fuel composition. Consequently, the NH_3 ratio is posited to fully encapsulate the sensitivity otherwise attributed to the H2 ratio.

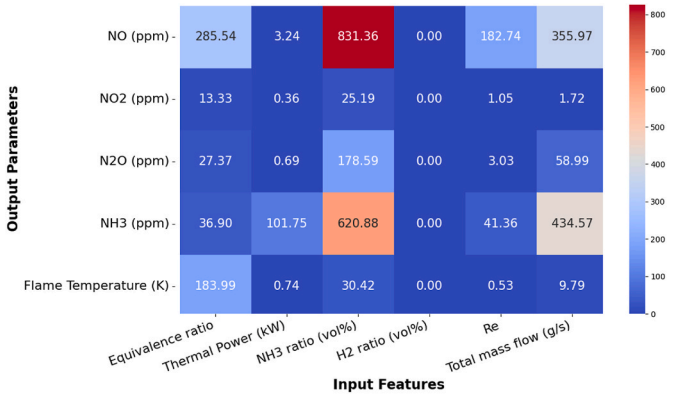

Fig. 7. Feature importance values computed via the perturbation-based method. Each value represents the average increase in MSE after randomly permuting the corresponding feature.

Overall, the heatmap accentuates the profound influence of the NH_3 ratio and equivalence ratio on emissions and AFT. Concurrently, it delineates the varying degrees of impact exerted by other input features on specific emissions—for instance, the total mass flow is identified as a significant determinant of emissions such as NO, NH_3, and N_2O. These discerned patterns furnish valuable insights for the optimization of combustion processes, aligning them with stringent environmental standards.

In light of the sensitivity analysis outcomes in Fig. 7 and the demonstrated efficacy of the XGBoost + SVR model in Table 9, this investigation further explores a feature importance analysis. This analysis is pivotal in discerning the individual contributions of input variables to the overall NOx emissions, thereby informing operational strategies and emission control for NH_3/H_2 combustion. Table 10 enumerates the significance of various input features as appraised by both the hybrid XGBoost + SVR and the standalone XGBoost models. The findings from both models concur that the NH_3 mole fraction, equivalence ratio, and total mass flow rate are paramount contributors to NOx emissions, aligning with the inferences of prior NH_3/H_2 combustion research [48,49]. The accumulative importance of the input features are shown in Fig. 8.

The observed shifts in feature importance from the standalone XGBoost to the XGBoost + SVR hybrid underscore the nuanced interaction effects that the SVR captures, which may elude the XGBoost model when operating in isolation. The pronounced impact of the NH_3 proportion within the hybrid model intimates a complex, non-linear interplay with the target variable, adeptly harnessed by the SVR. This complexity likely stems from the SVR proficiency in modeling intricate relationships between the residuals of XGBoost predictions and the target variable, relationships that are not immediately discernible within the primary XGBoost framework. Conversely, the negligible influence of the H_2 ratio in both models can be attributed to its functional redundancy relative to the NH_3 ratio. Furthermore, the disparate significance of the equivalence ratio and Reynolds number between the models suggests that their associations with the output variables are more linear, hence sufficiently captured by XGBoost, while the SVR does not contribute additional interpretive value for these variables.

4.3. Optimization of nitrogen emissions using the XSN framework

Given the detrimental impact of reactive nitrogen compounds on ecosystems—manifesting as air pollution and contributing to the greenhouse effect—and their adverse effects on human health, it is imperative to mitigate the concentration of total nitrogenous gases (NO,

Table 10
Importance of individual features across different models.

Model	Equivalence ratio	Thermal Power (kW)	NH_3 Ratio	H_2 Ratio	Re	Total Mass Flow (g/s)
XGBoost	0.3037	0.0252	0.2621	0.0000	0.2901	0.1197
XGBoost + SVR	0.0939	0.0076	0.6460	0.0000	0.0404	0.2122

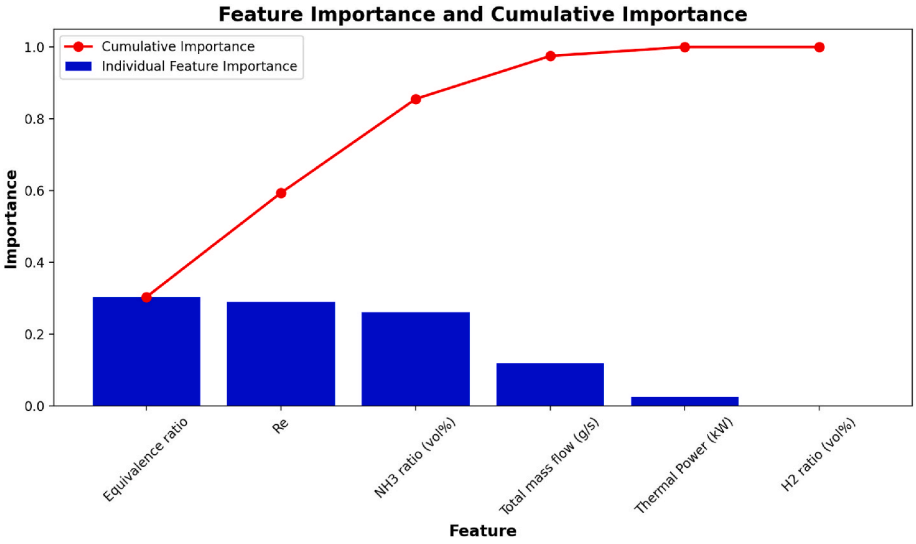

Fig. 8. Analysis of individual feature importance and cumulative importance based on XGBoost + SVR.

NO_2, N_2O, NH_3) in exhaust emissions. This necessitates the strategic modification of operating parameters within the swirl burner. After the establishment of the XGBoost + SVR model, which predicts NOx and NH_3 emissions as well as AFT under varying conditions and input features, the XSN framework is employed to optimize the selection of input features. The aim is to minimize nitrogen compounds while maintaining the AFT within the normal temperature range of 1600–2100 K based on the experimental dataset.

Table 11 delineates the input parameters alongside the nitrogen emissions and AFT for both the optimized model and the experimental setup with the lowest recorded nitrogen emissions. The empirical data indicated a minimum total nitrogen gas concentration of 69.81 ppm, whereas the optimization approach achieved a significant reduction to 33.57 ppm, marking a decrease of 51.91 %. This substantial diminution underscores the efficacy of the optimization model in regulating nitrogen emissions. Concurrently, the AFT is maintained at a viable 2013.66 K. Pertaining to the input features of the optimized data set, the equivalence ratio is established at 1.22 with an ammonia proportion of 95 %, figures that resonate with those derived from preceding NOx emission studies [50,51].

The Pareto front generated by the NSGA-II optimization delineates the complex interplay between NOx emissions, quantified through MSE values, and temperature discrepancies. As illustrated in Fig. 9, a well-

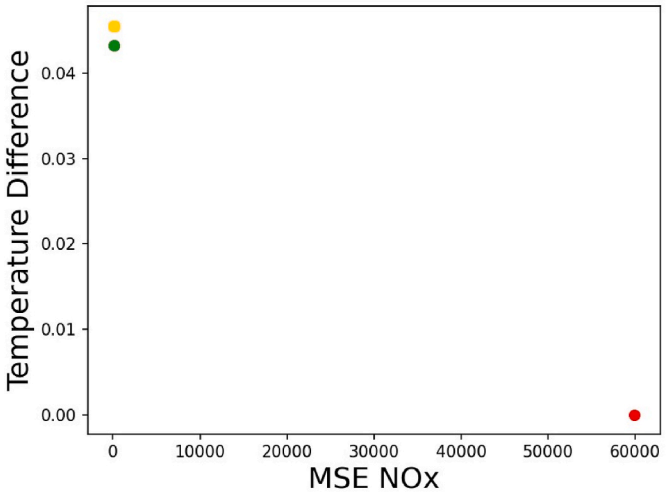

Fig. 9. Pareto front analysis: balancing NOx emissions and temperature variations in NH_3/H_2 combustion.

Table 11
Comparison between optimized and experimental value parameters.

Optimization model				Experimental data			
Input Features		Emissions		Input Features		Emissions	
Equivalence Ratio	1.25	**NO (ppm)**	19.50	**Equivalence Ratio**	1.15	**NO (ppm)**	58.00
Thermal Power (kW)	8.22	**NO_2 (ppm)**	8.10	**Thermal Power (kW)**	8.00	**NO_2 (ppm)**	6.74
NH_3 Ratio	0.95	**N_2O (ppm)**	4.17	**NH_3 Ratio**	0.75	**N_2O (ppm)**	2
H_2 Ratio	0.05	**NH_3 (ppm)**	1.80	**H_2 Ratio**	0.25	**NH_3 (ppm)**	3.07
Re	43447.59	**AFT (K)**	2013.66	**Re**	27029.66	**AFT (K)**	2032.93
Total Mass Flow (g/s)	2.80	**Total Nitrogen Emissions (ppm)**	33.57	**Total Mass Flow (g/s)**	2.58	**Total Nitrogen Emissions (ppm)**	69.81

defined clustering of solutions emerges, demonstrating the algorithm's capability to simultaneously minimize NOx emissions while maintaining controlled temperature fluctuations. The color-coded points highlight key trade-offs: solutions in the upper left region achieve significantly lower NOx MSE but with greater temperature deviations, whereas points in the lower right prioritize minimal temperature differences at the cost of higher NOx error. This distribution underscores the inherent trade-offs in combustion optimization, where minimizing one objective often necessitates compromises in the other. The presence of distinct solution clusters suggests that the algorithm effectively explores and exploits the search space, yielding multiple viable alternatives for decision-makers to select from based on operational priorities.

Fig. 10 further illustrates the evolutionary trajectory of the NSGA-II optimization over 50 generations, capturing the convergence behavior of NOx emissions and temperature differences. Initially, the fitness values exhibit considerable dispersion, indicative of broad exploratory sampling. As the algorithm progresses, both objectives exhibit a clear trend toward convergence, with NOx emissions and temperature deviations stabilizing into lower, more refined regions. The structured stratification observed in the scatter plots suggests that the algorithm efficiently identifies and retains high-quality solutions, progressively refining the Pareto set over successive generations. This convergence pattern is a testament to the optimization method's effectiveness in handling multi-objective trade-offs, demonstrating its capability to balance environmental constraints with operational feasibility. Overall, the results underscore the effectiveness of NSGA-II in handling this multi-objective optimization problem: it substantially reduces NOx emissions while maintaining controlled temperature variations. The algorithm not only finds a diverse set of optimal trade-off solutions, but it also does so with apparent efficiency, giving confidence that the obtained Pareto front is both representative and practical for informing real-world engineering decisions.

Notably, as shown in Table 11, the optimal condition corresponds to an NH_3 mole fraction of approximately 95 %, which is higher than typical experimental test cases. This outcome can be understood from both combustion science and optimization perspectives. High ammonia content results in lower flame temperature and reduced thermal NO_x, and by jointly optimizing equivalence ratio and mass flow rate, the model found a condition where most NH_3 is consumed, minimizing both NO_x and NH_3 slip. From a modeling standpoint, the genetic algorithm effectively explored the parameter space and determined that a small fraction of H_2 is sufficient for combustion stability, while excessive H_2 would have raised temperatures and increased NO_x formation. The result demonstrates the model's capacity to identify non-obvious but physically valid solutions through data-driven optimization.

4.4. Limitations and future work

While this study provides insights into multiple optimization objectives using NSGA-II, it is important to note a few considerations. The dataset employed is highly specific and proprietary, which could affect the generalizability of the findings to other settings or conditions where similar data are unavailable. Additionally, the computational demand of the NSGA-II algorithm, particularly with large dataset and complex models, is notable. This aspect might influence the applicability of the approach in scenarios where computational resources are constrained.

To address these limitations, future work can focus on enhancing the robustness and applicability of the study. First, collaborating with industry partners to obtain more extensive data or generate synthetic dataset can help validate and improve the model under different conditions. Second, conducting scalability studies to evaluate the performance of the proposed model under varying computational loads can ensure its applicability in different operating environments. Finally, future studies can explore integrating the developed model with a real-time monitoring system to dynamically optimize emissions based on changing operating conditions. Furthermore, to maximize its societal impact, future efforts should broaden the application of this tool to facilitate the transition towards net-zero emissions across critical energy sectors, including transportation and the built environment.

5. Conclusions

The urgency of mitigating climate change has propelled the search for clean energy alternatives, with hydrogen and ammonia emerging as frontrunners. Ammonia, in particular, shows promise due to its zero-carbon emissions and high energy density. Despite its potential, challenges such as a high ignition point and low reactivity pose barriers to its adoption as a fuel source. Ammonia/hydrogen blends offer a solution, yet they may increase NOx emissions. This study explores the optimization of operating parameters to reduce nitrogen emissions, combining the machine learning techniques, XGBoost and SVR, to improve prediction accuracy and reduce overfitting risks. The NSGA-II genetic algorithm is utilized to optimize model parameters, aiming to minimize nitrogen compounds in exhaust emissions. The main conclusions are listed as follows.

1. The XGBoost + SVR model demonstrates high predictive accuracy, with most R^2 values exceeding 0.97, indicating strong correlations between predicted and measured data. The exception is NO_2 with an (R^2) value of 0.934, likely due to its more scattered distribution and lower values.
2. When compared to other models like RF, ANN, and their combinations, the XGBoost + SVR model excels, achieving the lowest MSE (3508.31) and the highest R^2 value (0.97653). The superior performance of this hybrid model is credited to its ability to capture complex data patterns, with XGBoost addressing data variance and SVR modeling non-linear residuals.

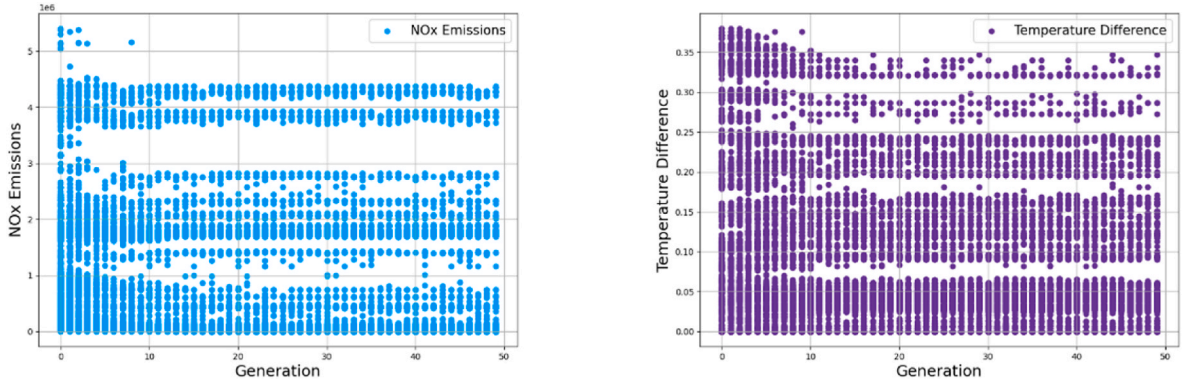

Fig. 10. Convergence of NOx emissions and temperature discrepancies over generations.

3. The feature importance analysis reveals that NH_3 mole proportion, equivalence ratio, and total mass flow rate are significant contributors to nitrogenous emissions (NO, NO_2, N_2O, and NH_3). The H_2 ratio appears to have a negligible impact, possibly due to its redundancy with the NH_3 ratio. The XGBoost model effectively captures the linear relationships of features like the equivalence ratio and Reynolds number, while the SVR does not add explanatory value for these features.
4. The proposed XSN framework successfully minimizes nitrogen compounds, reducing the total concentration of N-gases (NO, NO_2, N_2O, and NH_3) from 69.81 ppm to 33.57 ppm, a decrease of 51.91 %. The input features of the optimization model, such as an equivalence ratio of 1.22 and an ammonia proportion of 95 %, align closely with previous NOx emission studies, confirming the model's effectiveness in controlling nitrogen emissions.

CRediT authorship contribution statement

Hao Shi: Writing – original draft, Methodology, Formal analysis, Conceptualization. **Zebang Liu:** Writing – original draft, Methodology, Formal analysis, Conceptualization. **Syed Mashruk:** Validation, Investigation, Data curation. **Mohammad Alnajideen:** Validation, Conceptualization. **Ali Alnasif:** Validation, Investigation, Data curation. **Jing Liu:** Validation, Methodology, Formal analysis, Conceptualization. **Agustin Valera-Medina:** Writing – review & editing, Supervision, Resources, Project administration, Funding acquisition.

Declaration of competing interest

This statement is to certify that all authors have seen and approved the manuscript being submitted, and there is no conflict of interests. We warrant that the article is the authors' original work. We warrant that the article has not received prior publication and is not under consideration for publication elsewhere. On behalf of all Co-Authors, the corresponding Author shall bear full responsibility for the submission.

This research has not been submitted for publication nor has it been published in whole or in part elsewhere. We attest to the fact that all Authors listed on the title page have contributed significantly to the work, have read the manuscript, attest to the validity and legitimacy of the data and its interpretation, and agree to its submission to the Journal of *Energy*.

All authors agree that author list is correct in its content and order and that no modification to the author list can be made without the formal approval of the Editor-in-Chief, and all authors accept that the Editor-in-Chief's decisions over acceptance or rejection or in the event of any breach of the Principles of Ethical Publishing in the Journal of *Energy* being discovered of retraction are final.

Acknowledgements

This work was supported by the SAFE-AGT pilot (no. EP/T009314/1) funded by the Engineering and Physical Sciences Research Council (EPSRC). The research was undertaken at Cardiff University's Thermofluids Lab with invaluable technical support from Mr. Malcolm Seaborne.

Data availability

Data will be made available on request.

References

[1] A IE. World energy outlook 2022. France: IEA Paris; 2022.
[2] Woon KS, Phuang ZX, Taler J, Varbanov PS, Chong CT, Klemeš JJ, et al. Recent advances in urban green energy development towards carbon emissions neutrality. Energy (Calg) 2023;267:126502.
[3] Papadis E, Tsatsaronis G. Challenges in the decarbonization of the energy sector. Energy (Calg) 2020;205:118025.
[4] Shi H, Mashruk S, Alnajideen M, Valera-Medina A. Combustion systems for ammonia-fuelled gas turbines and other propulsion devices. IET; 2024.
[5] Valera-Medina A, Vigueras-Zuniga MO, Shi H, Mashruk S, Alnajideen M, Alnasif A, et al. Ammonia combustion in furnaces: a review. Int J Hydrogen Energy 2024;49:1597–618.
[6] Shi H, Boulet E, Dong D, Alnajideen M, Mashruk S, Zhang Z, et al. Ammonia-fueled internal combustion engines. 2024.
[7] Chen J, Jiang X, Qin X, Huang Z. Effect of hydrogen blending on the high temperature auto-ignition of ammonia at elevated pressure. Fuel (Guildf) 2021;287:119563.
[8] Lhuillier C, Brequigny P, Contino F, Mounaïm-Rousselle C. Experimental study on ammonia/hydrogen/air combustion in spark ignition engine conditions. Fuel (Guildf) 2020;269:117448.
[9] Zhang H, Lei N, Wang Z. Ammonia-hydrogen propulsion system for carbon-free heavy-duty vehicles. Appl Energy 2024;369:123505.
[10] Mashruk S, Shi H, Zitouni S-E, Valera-Medina A. Nitrogen oxide emissions in ammonia combustion. Ammonia and hydrogen for green energy transition. Springer; 2024. p. 289–328.
[11] Lee S, Kwon OC. Effects of ammonia substitution on extinction limits and structure of counterflow nonpremixed hydrogen/air flames. Int J Hydrogen Energy 2011;36:10117–28.
[12] Otomo J, Koshi M, Mitsumori T, Iwasaki H, Yamada K. Chemical kinetic modeling of ammonia oxidation with improved reaction mechanism for ammonia/air and ammonia/hydrogen/air combustion. Int J Hydrogen Energy 2018;43:3004–14.
[13] Shi C, Zhang Z, Wang H, Wang J, Cheng T, Zhang L. Parametric analysis and optimization of the combustion process and pollutant performance for ammonia-diesel dual-fuel engines. Energy (Calg) 2024;296:131171.
[14] Nakamura K, Muramatsu T, Ogawa T, Nakagaki T. Prediction of de-NOx performance using monolithic SCR catalyst under load following operation of natural gas-fired combined cycle power plants. Energy (Calg) 2021;227:120383.
[15] Mashruk S, Xiao H, Valera-Medina A. Rich-Quench-Lean model comparison for the clean use of humidified ammonia/hydrogen combustion systems. Int J Hydrogen Energy 2021;46:4472–84.
[16] Lin Q, Jiang Y, Liu C, Chen L, Zhang W, Ding J, et al. Controllable NO emission and high flame performance of ammonia combustion assisted by non-equilibrium plasma. Fuel (Guildf) 2022;319:123818.
[17] Zhou L, Song Y, Ji W, Wei H. Machine learning for combustion. Energy AI 2022;7:100128.
[18] Sun P, Zhang J, Dong W, Li D, Yu X. Prediction of oxygen-enriched combustion and emission performance on a spark ignition engine using artificial neural networks. Appl Energy 2023;348:121466.
[19] Adewole BZ, Abidakun OA, Asere AA. Artificial neural network prediction of exhaust emissions and flame temperature in LPG (liquefied petroleum gas) fueled low swirl burner. Energy (Calg) 2013;61:606–11.
[20] Lopes C, Perdigão F. Event detection by HMM, SVM and ANN: a comparative study. Computational processing of the Portuguese language: 8th international conference, PROPOR 2008 Aveiro, Portugal. September 8-10, 2008 proceedings 8. Springer; 2008. p. 1–10.
[21] Wei Z, Li X, Xu L, Cheng Y. Comparative study of computational intelligence approaches for NOx reduction of coal-fired boiler. Energy (Calg) 2013;55:683–92.
[22] 23-Random forests [n.d].
[23] Udaybhanu G, Jameel AGA, Roberts WL, Reddy VM. Development of laminar burning velocity prediction model and correlation of iso-octane air mixtures using artificial neural network. Energy (Calg) 2024;307:132639.
[24] Kubal C, Haase D, Meyer V, Scheuer S. Integrated urban flood risk assessment–adapting a multicriteria approach to a city. Nat Hazards Earth Syst Sci 2009;9:1881–95.
[25] Ye T, Dong M, Long J, Zheng Y, Liang Y, Lu J. Multi-objective modeling of boiler combustion based on feature fusion and Bayesian optimization. Comput Chem Eng 2022;165:107913.
[26] Yan P, Fan W, Zhang R. Predicting the NOx emissions of low heat value gas rich-quench-lean combustor via three integrated learning algorithms with Bayesian optimization. Energy (Calg) 2023;273:127227.
[27] Li G, Li W, Tian X, Che YF. Short-term electricity load forecasting based on the XGBoost algorithm. Smart Grid 2017;7:274–85.
[28] Dong Y, Mao D, Zhang M. Research on optimization and adjustment of gas turbine combustion based on XGBoost and NSGA-II. 2021 6th international conference on power and renewable energy (ICPRE). IEEE; 2021. p. 1512–8.
[29] Yao S, Kronenburg A, Stein OT. Efficient modeling of the filtered density function in turbulent sprays using ensemble learning. Combust Flame 2022;237:111722.
[30] Zhong H, Wang J, Jia H, Mu Y, Lv S. Vector field-based support vector regression for building energy consumption prediction. Appl Energy 2019;242:403–14.
[31] Koley S. Electrochemistry of phase-change materials in thermal energy storage systems: a critical review of green transitions in built environments. Trends Sci 2024;21:8538.
[32] Wong KI, Wong PK, Cheung CS, Vong CM. Modeling and optimization of biodiesel engine performance using advanced machine learning methods. Energy (Calg) 2013;55:519–28.
[33] Jin N, Guo L, Liu X. Machine learning-aided optimization of coal decoupling combustion for lowering NO and CO emissions simultaneously. Comput Chem Eng 2022;162:107822.
[34] Rahat AAM, Wang C, Everson RM, Fieldsend JE. Data-driven multi-objective optimisation of coal-fired boiler combustion systems. Appl Energy 2018;229:446–58.

[35] Zhang L, Ge H, Ma Y, Xue J, Li H, Pecht M. Multi-objective optimization design of a notch filter based on improved NSGA-II for conducted emissions. IEEE Access 2020;8:83213–23.
[36] Kwon E, Ahn J, Cho B, Park D. A study on development of recycled cement made from waste cementitious powder. Constr Build Mater 2015;83:174–80.
[37] Sato D, Davies J, Mazzotta L, Mashruk S, Valera-Medina A, Kurose R. Effects of reynolds number and ammonia fraction on combustion characteristics of premixed ammonia-hydrogen-air swirling flames. Proc Combust Inst 2024;40:105283.
[38] Mashruk S, Shi H, Mazzotta L, Ustun CE, Aravind B, Meloni R, et al. Perspectives on NO X emissions and impacts from ammonia combustion processes. Energy Fuels 2024;38:19253–92.
[39] Dandy David. Transport properties calculator n.d. https://navier.engr.colostate.edu/code/code-2/index.html (accessed March 11, 2025)..
[40] Stagni A, Cavallotti C, Arunthanayothin S, Song Y, Herbinet O, Battin-Leclerc F, et al. An experimental, theoretical and kinetic-modeling study of the gas-phase oxidation of ammonia. React Chem Eng 2020;5:696–711.
[41] Mashruk S, Zitouni S-E, Brequigny P, Mounaim-Rousselle C, Valera-Medina A. Combustion performances of premixed ammonia/hydrogen/air laminar and swirling flames for a wide range of equivalence ratios. Int J Hydrogen Energy 2022;47:41170–82.
[42] Alnasif A, Mashruk S, Kovaleva M, Wang P, Valera-Medina A. Experimental and numerical analyses of nitrogen oxides formation in a high ammonia-low hydrogen blend using a tangential swirl burner. Carbon Neutral 2022;1:24.
[43] Chen T, Guestrin C. Xgboost: a scalable tree boosting system. In: Proceedings of the 22nd acm sigkdd international conference on knowledge discovery and data mining; 2016. p. 785–94.
[44] Han Z, Hossain MM, Wang Y, Li J, Xu C. Combustion stability monitoring through flame imaging and stacked sparse autoencoder based deep neural network. Appl Energy 2020;259:114159.
[45] Deb K, Pratap A, Agarwal S, Meyarivan T. A fast and elitist multiobjective genetic algorithm: NSGA-II. IEEE Trans Evol Comput 2002;6:182–97.
[46] Zhou H, Zheng L, Cen K. Computational intelligence approach for NOx emissions minimization in a coal-fired utility boiler. Energy Convers Manag 2010;51:580–6.
[47] Mashruk S, Okafor EC, Kovaleva M, Alnasif A, Pugh D, Hayakawa A, et al. Evolution of N2O production at lean combustion condition in NH3/H2/air premixed swirling flames. Combust Flame 2022;244:112299.
[48] Li Z, Li S. Kinetics modeling of NOx emissions characteristics of a NH3/H2 fueled gas turbine combustor. Int J Hydrogen Energy 2021;46:4526–37.
[49] Cai T, Zhao D. Effects of fuel composition and wall thermal conductivity on thermal and NOx emission performances of an ammonia/hydrogen-oxygen micro-power system. Fuel Process Technol 2020;209:106527.
[50] Mashruk S, Kovaleva M, Alnasif A, Chong CT, Hayakawa A, Okafor EC, et al. Nitrogen oxide emissions analyses in ammonia/hydrogen/air premixed swirling flames. Energy (Calg) 2022;260:125183.
[51] Rocha RC, Costa M, Bai X-S. Combustion and emission characteristics of ammonia under conditions relevant to modern gas turbines. Combust Sci Technol 2021;193:2514–33.